Vol 13 No 6, June 2004
1009-1963/2004/13(06)/0898-07

Chinese Physics

© 2004 Chin. Phys. Soc.
and IOP Publishing Ltd

Study of electron temperature gradient instability in toroidal plasmas with negative magnetic shear*

Jian Guang-De(简广德)† and Dong Jia-Qi(董家齐)

Southwestern Institute of Physics, Chengdu 610041, *China*

(Received 23 September 2003; revised manuscript received 6 February 2004)

Electron temperature gradient driven instability in toroidal plasmas with negative magnetic shear is studied. Full electron kinetics is considered, and the behaviours of the modes and corresponding turbulent transport in the parameter regimes close to the instability threshold are emphasized. Growing and damped modes are both investigated. The singular points of the integrand are disposed of, and the fitting formulae for the critical gradient are given. The theoretical results are shown to be close to the experimental observations.

Keywords: electron temperature gradient instability, critical gradient, negative magnetic shear
PACC: 5235P, 5255G, 5265

1. Introduction

Understanding and controlling the anomalous transport observed experimentally on tokamak devices is one of the major challenges for magnetic confinement fusion research. There is strong experimental evidence that such anomaly may be attributed to a variety of small scale turbulence driven by gradients of plasma parameters such as density, velocity or temperature.[1] The observations on tokamaks have shown that, within internal transport barriers (ITBs), electron thermal transport hardly changes while ion thermal diffusivity was reduced to the neoclassical level. These findings support the hypothesis that, within an ITB, ion temperature gradient (ITG) turbulence is suppressed by $E \times B$ shear flow, whereas electron temperature gradient (ETG) turbulence controls the electron transport. Therefore, it is accepted in the plasma physics community that linear and nonlinear ITG instability theories and simulations are enough to explain the ion transport anomaly qualitatively.

In recent years, ETG instability and anomalous electron thermal transport has become a hot topic and received extensive research attention.[2−10]

The correlation of ETG turbulence and the electron thermal transport was studied with quasi-linear theory in a sheared slab geometry in the 1980s.[2,3] The formula for electron conductivity introduced in these works successfully explained the so-called electron temperature profile consistency observed in experiments. In addition, the formula was improved with the inclusion of toroidal effects.[4] Recently, the correlation of ETG turbulence and the electron thermal transport was studied with gyro-kinetic nonlinear simulation.[5,6] Furthermore, the critical temperature gradients for the ETG instability and electron transport were studied experimentally [11−14] and theoretically.[9]

In this paper, the ETG instability and corresponding turbulent transport in toroidal plasmas with negative magnetic shear is studied using the integral eigenvalue equations.[15] The full electron kinetics is considered and the behaviours of the modes and the transport in the parameter regimes close to the instability threshold are emphasized. A new integral scheme is introduced in this work,[16] which allows the study of both growing and damped modes. Therefore, the critical gradients are accurately calculated without extrapolation, which, generally speaking, is usually less accurate.

The singular points of the integrand are disposed of. The fitting formulae of the critical gradient, for negative magnetic shear, are given.

*Project supported by the National Natural Science Foundation of China (Grant No 10135020).
†E-mail: gdjian@swip.ac.cn

2. Integral eigenmode equations

Suppressing the compressional Alfvèn waves, the dynamics of low-frequency electromagnetic perturbation in inhomogeneous low-β (β=plasma pressure/magnetic pressure) plasmas is described by the quasi-neutrality condition

$$\tilde{n}_{\rm e} = \tilde{n}_{\rm i}, \tag{1}$$

and by the parallel component of Ampère's law

$$\nabla_\perp^2 \tilde{A}_{//} = -\frac{4\pi}{c}\tilde{j}_{\rm i//} - \frac{4\pi}{c}\tilde{j}_{\rm e//}. \tag{2}$$

Here, the perturbed particle density $\tilde{n}_s$ is given by

$$\tilde{n}_s = \int {\rm d}^3 v\ f_s, \tag{3}$$

while the parallel component of perturbed current density from the electrons and ions are given by

$$\tilde{j}_{s//} = q_s \int v_{//} f_s {\rm d}^3 v, \tag{4}$$

with

$$f_s = -\frac{q_s F_{{\rm M}s}}{T_s}\tilde{\phi} + h_s J_0(\delta_s), \quad \text{for} \quad s = {\rm i, e}. \tag{5}$$

The non-adiabatic response h_s is determined by solving the gyro-kinetic equation in ballooning space,

$$\begin{aligned} &{\rm i}\frac{v_{//}}{Rq}\frac{\partial}{\partial\theta}h_s + (\omega - \omega_{Ds})h_s \\ =&(\omega - \omega_{*s{\rm T}}){\rm J}_0(\delta_s)F_{{\rm M}s}\frac{q_s n_0}{T_s} \\ &\times\left(\hat{\phi}(\theta) - \frac{v_{//}}{c}\hat{A}_{//}(\theta)\right), \end{aligned} \tag{6}$$

where

$$\omega_{{\rm D}s} = 2\varepsilon_n\omega_{*s}[\cos\theta + \sin\theta\hat{s}\theta - \alpha\sin\theta)]\left(\frac{\hat{v}_\perp^2}{2} + \hat{v}_{//}^2\right),$$

$$\omega_{*s{\rm T}} = \omega_{*s}\left[1 + \eta_s\left(\frac{v^2}{v_{ts}^2} - \frac{3}{2}\right)\right],$$

$$F_{{\rm M}s} = (\pi v_{ts}^2)^{-3/2}\exp(-v^2/v_{ts}^2),$$

where $\rm J_0$ is the Bessel function of zero-order and $\delta_s = (2b_s)^{1/2}v_\perp$, $2b_s = k_\perp^2 v_{ts}^2/\Omega_s^2$, $v_{ts}^2 = 2T_s/m_s$, $\omega_{*s} = ck_\theta T_s/q_s B L_n$ and $\Omega_s = q_s B/m_s c$ are the diamagnetic drift frequency and the gyro-frequency of species s=(i,e), respectively. We note that the well-known ballooning representation,

$$\tilde{f} = \sum_{-\infty}^{\infty}{\rm e}^{{\rm i}m\theta}\int_{-\infty}^{\infty}{\rm e}^{-{\rm i}m\theta'}{\rm e}^{-{\rm i}n(\varsigma - q\theta') - {\rm i}\omega t}\tilde{f}_n(\theta'){\rm d}\theta', \tag{7}$$

with ς and θ' being the toroidal and extended poloidal angles respectively, has been used in deriving Eq.(6), and the s-α equilibrium model with circular flux surfaces has also been employed.

Equation (6) can be easily integrated with the boundary condition $h_s(\theta) = 0$ as $\theta \to \pm{\rm sgn}(v_{//})_\infty$.

The perturbed particle and current densities are obtained from Eqs.(3) and (4) as follows:

$$\begin{aligned} \hat{n}_{\rm e}(k) =&\frac{ne}{T_{\rm e}}\hat{\phi}(k) - \frac{ne}{T_{\rm e}}\int_{-\infty}^{\infty}\frac{{\rm d}k'}{\sqrt{2\pi}}\{K_{11}(k,k')\hat{\phi}(k') \\ &+ K_{12}(k,k')\hat{A}_{//}(k')\}, \end{aligned} \tag{8}$$

$$\begin{aligned} \hat{j}_{e//}(k) =&-\frac{ne^2 c_s\sqrt{2\tau_{\rm i}}}{T_{\rm e}\beta_{\rm i}}\int_{-\infty}^{\infty}\frac{{\rm d}k'}{\sqrt{2\pi}}\{K_{21}(k,k')\hat{\phi}(k') \\ &+ K_{22}(k,k')\hat{A}_{//}(k')\}. \end{aligned} \tag{9}$$

Substituting Eqs.(8), (9) into the quasi-neutrality condition, Eq.(1), and the parallel component of Ampère's law, Eq.(2), we can straightforwardly derive the following two coupled integral eigenmode equations:

$$\begin{aligned} \left[1 + \tau_{\rm i} + \frac{k_\perp^2}{2}\frac{\Omega_{\rm e}^2}{\omega_{\rm pe}^2}\right]\hat{\phi}(k) =&\int_{-\infty}^{\infty}\frac{{\rm d}k'}{\sqrt{2\pi}}\{K_{11}(k,k')\hat{\phi}(k') \\ &+ K_{12}(k,k')\hat{A}_{//}(k')\}, \end{aligned} \tag{10}$$

$$\begin{aligned} \frac{1}{2}k_\perp^2\hat{A}_{//}(k) =&\int_{-\infty}^{\infty}\frac{{\rm d}k'}{\sqrt{2\pi}}\{K_{21}(k,k')\hat{\phi}(k') \\ &+ K_{22}(k,k')\hat{A}_{//}(k')\}, \end{aligned} \tag{11}$$

where $\hat{\phi}(k)$ and $\hat{A}_{//}(k)$ are the extended Fourier components (in ballooning space) of $\tilde{\phi}(r)$ and $(v_{\rm te}/c)\tilde{A}_{//}(r)$, and

$$K_{ij}(k,k') = -{\rm i}\int_{-\infty}^{0}\omega_{*{\rm e}}{\rm d}\tau H_{ij}(k,k'), \tag{12}$$

for i=1, 2, and j=1, 2. Here,

$$\begin{aligned} H_{11}(k,k') =&\sqrt{2}{\rm e}^{-{\rm i}\omega\tau}\frac{\exp\left[-\dfrac{(k'-k)^2}{4\lambda_{\rm e}}\right]}{\sqrt{a_{\rm e}}(1+a_{\rm e})\sqrt{\lambda_{\rm e}}} \\ &\times\left\{D_0 - \frac{\eta_{\rm e}(k-k')^2}{4a_{\rm e}\lambda_{\rm e}}\right\}\Gamma_0(k_\perp, k'_\perp), \end{aligned} \tag{13}$$

$$\begin{aligned} D_0 =&\frac{\omega}{\omega_{*{\rm e}}} - 1 + \frac{3}{2}\eta_{\rm e} - \frac{2\eta_{\rm e}}{1+a_{\rm e}} \\ &\times\left[1 - \frac{k_\perp^2 + k'^2_\perp}{2(1+a_{\rm e})} + \frac{k_\perp k'_\perp {\rm I}_1}{(1+a_{\rm e}){\rm I}_0}\right], \end{aligned} \tag{14}$$

$$H_{12}(k,k') = -\frac{1}{2\sqrt{a_{\rm e}\lambda_{\rm e}}}(k-k')H_{11}(k,k'), \tag{15}$$

$$H_{21}(k,k') = \frac{\beta_{\rm e}}{2\sqrt{a_{\rm e}\lambda_{\rm e}}}(k-k')H_{11}(k,k'), \tag{16}$$

$$H_{22}(k,k') = -\frac{\beta_{\rm e}}{4a_{\rm e}\lambda_{\rm e}}(k-k')^2 H_{11}(k,k'), \qquad (17)$$

with

$$\lambda_{\rm e} = \frac{\tau^2\omega_{*\rm e}^2}{a_{\rm e}}\left(\frac{\hat{s}}{q}\varepsilon_n\right)^2,$$
$$a_{\rm e} = 1 - {\rm i}2\varepsilon_n\omega_{*\rm e}\tau\frac{g(\theta,\theta')}{\theta-\theta'}.$$

Here

$$g(\theta,\theta') = (\hat{s}+1)(\sin\theta - \sin\theta') - \hat{s}(\theta\cos\theta - \theta'\cos\theta') - \frac{\alpha}{2}(\theta - \theta' - \sin\theta\cos\theta + \sin\theta'\cos\theta'),$$

$$\alpha = -R_0 q^2\frac{{\rm d}\beta}{{\rm d}r}$$
$$\beta = \beta_{\rm i} + \beta_{\rm e} = \beta_{\rm e}\left(1 + \frac{T_{\rm i}}{T_{\rm e}}\right),$$
$$\beta_{\rm e} = \frac{8\pi n T_{\rm e}}{B^2},$$
$$k = k_\theta\hat{s}\theta, \quad k' = k_\theta\hat{s}\theta',$$
$$\Gamma_0 = {\rm I}_0\left(\frac{k_\perp k'_\perp}{1+a_{\rm e}}\right)\exp\left[-(k_\perp^2 + k_\perp'^2)/2(1+a_{\rm e})\right],$$
$$k_\perp^2 = k_\theta^2[1 + (\hat{s}\theta - \alpha\sin\theta)^2],$$
$$k_\perp'^2 = k_\theta^2[1 + (\hat{s}\theta' - \alpha\sin\theta')^2],$$
$$\omega_{*\rm e} = \frac{cT_{\rm e}k_\theta}{eBL_n}, \quad \varepsilon_n = \frac{L_n}{R},$$
$$\eta_{\rm e} = \frac{L_n}{L_{\rm Te}}, \quad \tau_{\rm i} = \frac{T_{\rm e}}{T_{\rm i}}.$$

The quantities k, k' and k_θ are normalized to $\rho_{\rm e}^{-1} = eB/c\sqrt{2T_{\rm e}m_{\rm e}}$. ${\rm I}_j$ is the modified Bessel function of order j=0, 1. In addition, all the symbols have their usual meanings such as L_n is the density gradient scale length, $L_{\rm Te}$ is electron temperature gradient scale length, q is the safety factor, $\hat{s} = r{\rm d}q/q{\rm d}r$ is the magnetic shear and $\omega_{*\rm e} = cT_{\rm e}k_\theta/eBL_n$ is the electron diamagnetic drift frequency. The m and T are the masses and temperatures, respectively.

The pressure gradient parameter α is not independent and may be expressed with other parameters as

$$\alpha = -Rq^2\frac{{\rm d}\beta}{{\rm d}r} = \frac{q^2\beta_{\rm e}}{\varepsilon_n}(1 + \tau_{\rm i}^{-1} + \eta_{\rm e}). \qquad (18)$$

In the local approximation, the magnetic shear effects are neglected and the parallel wavevector $k_{//}$=const is used. From the Poisson equation and the parallel component of Ampère's law, we can straightforwardly derive the following two coupled eigenmode equations which are the reduced versions of Eqs.(10) and (11) in the local approximation:

$$\left[1 + \tau_{\rm i} + \frac{k_\perp^2}{2}\frac{\Omega_{\rm e}^2}{\omega_{\rm pe}^2} + P_0\right]\hat{\phi}(k) + P_1\hat{A}_{//}(k') = 0, \qquad (19)$$

$$-\beta_{\rm e}P_1\hat{\phi}(k) + \left[\frac{1}{2}k_\perp^2 + \beta_{\rm e}P_2\right]\hat{A}_{//}(k') = 0, \qquad (20)$$

where

$$P_0 = {\rm i}2\int_{-\infty}^{0}\omega_{*\rm e}{\rm d}\tau D_1 \times\left\{D_0 - \frac{\eta_{\rm e}}{a_{\rm e}}\left[\frac{1}{2} - \left(\frac{k_{//}v_{\rm te}\tau}{2\sqrt{a_{\rm e}}}\right)^2\right]\right\} \times\Gamma_0(k_\perp, k'_\perp), \qquad (21)$$

$$P_1 = -\int_{-\infty}^{0}\omega_{*\rm e}{\rm d}\tau\frac{k_{//}v_{\rm te}\tau}{a_{\rm e}}D_1 \times\left\{D_0 - \frac{\eta_{\rm e}}{a_{\rm e}}\left[\frac{3}{2} - \left(\frac{k_{//}v_{\rm te}\tau}{2\sqrt{a_{\rm e}}}\right)^2\right]\right\} \times\Gamma_0(k_\perp, k'_\perp), \qquad (22)$$

$$P_2 = -{\rm i}2\int_{-\infty}^{0}\omega_{*\rm e}{\rm d}\tau D_1\left[\left(\frac{1}{2} - \left(\frac{k_{//}v_{\rm te}\tau}{2\sqrt{a_{\rm e}}}\right)^2\right) \times\left\{D_0 - \frac{\eta_{\rm e}}{a_{\rm e}}\left[\frac{5}{2} - \left(\frac{k_{//}v_{\rm te}\tau}{2\sqrt{a_{\rm e}}}\right)^2\right]\right\} + \frac{\eta_{\rm e}}{2a_{\rm e}}\right] \times\Gamma_0(k_\perp, k'_\perp), \qquad (23)$$

$$D_1 = {\rm e}^{-{\rm i}\omega\tau}\frac{\exp\left[-\left(\frac{k_{//}v_{\rm te}\tau}{2\sqrt{a_{\rm e}}}\right)^2\right]}{\sqrt{a_{\rm e}}(1+a_{\rm e})}. \qquad (24)$$

Equations (19) and (20) are very useful for obtaining approximate results quickly in a limited computer time, while solving Eqs.(10) and (11) needs much more computer time for accurate results.

3. Method of solution

The coupled integral equations (10) and (11) have to be solved numerically. The numerical codes for the study of toroidal electrostatic [15] and sheared slab electromagnetic ITG modes [17] have been extended to investigate low-β electromagnetic eigenmodes in a torus. The computer code for solving the equations is upgraded by introducing a new scheme. The integration with respect to τ in Eq.(12) does not converge for damping modes with negative growth rate (imaginary part of ω) if it is performed along the real axis.

For the numerical results given in this work, we transform the real τ integration to an integration in a complex τ-plane with [16]

$$\tau = \begin{cases} -(1 + {\rm i}|\omega|s)s, & \omega_{\rm r} > 0, \\ -(1 - {\rm i}|\omega|s)s, & \omega_{\rm r} < 0, \end{cases} \qquad (25)$$

where $s(0 \le s < \infty)$ is a real integration variable.

It has been proved in Ref.[16] that the analytical continuation of the integration into the complex

τ-plane does not change the results of the integration and allows it to converge for a negative growth rate. Equations (10) and (11) are solved first with real and complex τ to check the correctness of the new numerical scheme implementation. It turns out that the new scheme allows not only the damping rate to be calculated but also a rapid convergence of the integration with high precision.

The integral eigenvalue equations are numerically solved with the Rayleigh–Ritz method. Generally, an eigenvalue problem can be written in the following form:

$$Kf = \lambda_0 f, \tag{26}$$

where K is a $2N \times 2N$ matrix, λ_0 is an eigenvalue, and f is the corresponding eigenfunction.

Now, we expand the approximate solution of Eqs.(10) and (11) in terms of unknown functions

$$\hat{\phi}_N = \sum_{j=1}^{N} b_j x_j(k), \tag{27}$$

and

$$\hat{A}_{//N} = \sum_{j=1}^{N} c_j x_j(k). \tag{28}$$

Substituting the above formulae into Eqs.(10) and (11), and integrating in k space, we can obtain a set of algebraic equations, which are based on the unknown quantity $a = (a_1, a_2, \ldots, a_{2N})^{\mathrm{T}}$

$$Ma = 0, \tag{29}$$

where M is a $2N \times 2N$ matrix, eigenvalue ω ($\mathrm{Re}\,\omega$ and $\mathrm{Im}\,\omega$ are the frequency and growth rate of mode) is determined by

$$\det[M_{ij}] = 0. \tag{30}$$

Double integrals with singular points have to be calculated in the matrix elements of M_{ij} (i, j=1, 2, $\ldots, 2N$). Two methods for dealing with the singularity of the integrand are discussed as follows.

(A) $\tau = 0$ and $k \neq k'$ case

In this case, $a_{\mathrm{e}} = 1$ and a singular point in the integrand occurs due to $\lambda_{\mathrm{e}} = \tau^2 \omega_{*\mathrm{e}}^2 \left(\frac{\hat{s}}{q}\varepsilon_n\right)^2$ in the denominator in Eq.(13). We can calculate the limit values of the following two expressions by L'Hospital's rule, then

$$\lim_{\tau \to 0} \frac{\exp\left[-(k'-k)^2/4\lambda_{\mathrm{e}}\right]}{\sqrt{\lambda_{\mathrm{e}}}} = 0, \tag{31}$$

$$\lim_{\tau \to 0} \frac{\exp\left[-(k'-k)^2/4\lambda_{\mathrm{e}}\right]}{\sqrt{\lambda_{\mathrm{e}}} \cdot \lambda_{\mathrm{e}}} = 0. \tag{32}$$

This means that the integrand value is zero when $\tau = 0$ and $k \neq k'$. The integral is calculated with Romberg's method of accelerating convergence, which saves computer time and has a higher accuracy.

(B) $\tau \neq 0$ and $k = k'$ case

The singularity may be eliminated using L'Hospital's rule,

$$\lim_{\theta \to \theta'} \frac{g(\theta, \theta')}{\theta - \theta'} = \lim_{\theta \to \theta'} \frac{(\hat{s}+1)\cos\theta - \hat{s}(\cos\theta - \theta\sin\theta)}{1} = (\hat{s}+1)\cos\theta' - \hat{s}(\cos\theta' - \theta'\sin\theta'). \tag{33}$$

In the calculation of the matrix elements, there are still two cases in which $\tau = 0$, $k = k'$ and $\tau \neq 0$, $k \neq k'$, besides the two cases mentioned above. The case of $\tau = 0$, $k = k'$ occurs in the calculation of the diagonal elements, and we can carry out the integration using the Gauss method. The case of $\tau \neq 0$, $k \neq k'$ is a normal integral without singularity, and we can perform the integration by Romberg's method of accelerating convergence.

4. Numerical results

The parameters for the numerical results given here are $\hat{s} = -1$, $q = 1.5$, $\tau_{\mathrm{i}} = 3$ and $d_s = \Omega_{\mathrm{e}}^2/\omega_{\mathrm{pe}}^2 = 0$ unless otherwise stated. These parameters are typical for tokamak plasmas in confinement regions.

4.1. Critical gradient versus toroidicity

Given in Fig.1, for $\hat{s} = 1$, is the maximum growth rate of the mode (with respect to k_θ) versus ETG parameter η_{e} and $R/L_{\mathrm{Te}} = \eta_{\mathrm{e}}/\varepsilon_n$, in the region close to the marginal stability boundary. The value $k_\theta \approx 0.3$ corresponds to the maximum growth rates for the chosen parameters. In Fig.1(a), the lines from left to right are for $\varepsilon_n = 0.1$ (the line with open circles), 0.2 (the line with solid circles), 0.3 (the line with open triangles), 0.4 (the line with solid triangles), 0.5 (the line with open squares), and 0.6 (the line with solid squares), respectively. The ε_n values for the lines in Fig.1(b) are not difficult to find if we keep in mind that the vertical axis here is the same as in Fig.1(a).

Given in Fig.2 is the maximum growth rate of the mode versus ETG for the same parameters as those in Fig.1, except $\hat{s} = -1$ here. In comparison with a positive magnetic shear of the same magnitude, we see that the slopes of the lines are smaller. The k_θ values, from 0.49 to 0.63, correspond to the maximum growth rates for the chosen parameters.

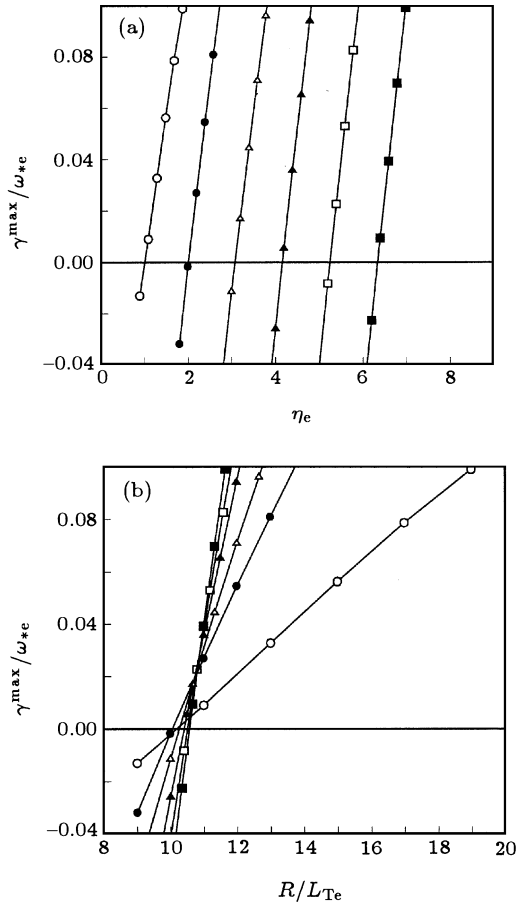


Fig.1. The maximum growth rate of the mode (with respect to k_θ) versus electron temperature gradient parameter η_e (a) and R/L_{Te} (b), for ε_n=0.1, 0.2, 0.3, 0.4, 0.5, 0.6, $\hat{s}$=1, q=1.5, τ_i=3, and Ω_e^2/ω_{pe}^2=0.

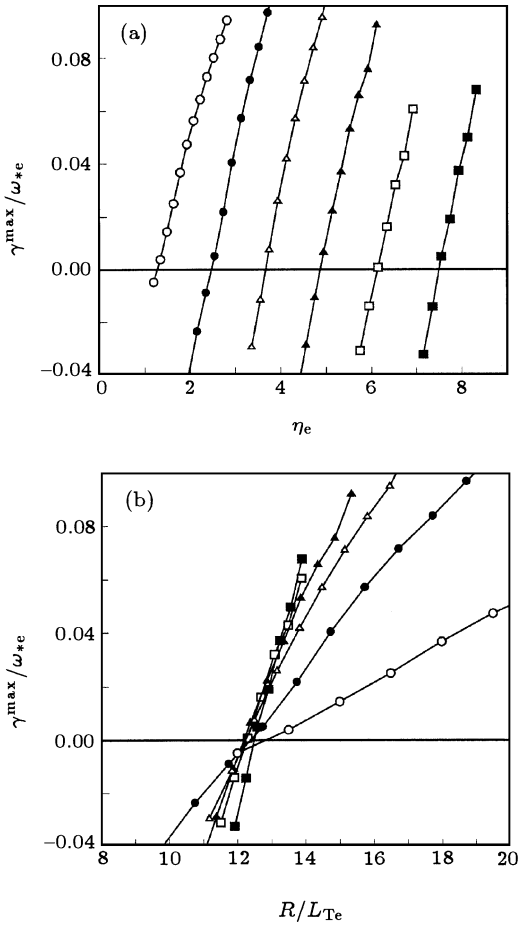


Fig.2. The maximum growth rate of the mode (with respect to k_θ) versus electron temperature gradient parameter η_e (a) and R/L_{Te} (b), for $\hat{s}=-1$, with other parameters being the same as in Fig.1.

From the numerical results, it is explicitly demonstrated that the maximum growth rate is an offset linear function of η_e,

$$\gamma^{\max} = \sigma^{ns}\omega_{*e}(\eta_e - \eta_e^{cns}), \tag{34}$$

or of R/L_{Te},

$$\gamma^{\max} = \sigma^{ns}\omega_{*e}\varepsilon_n\left[\frac{R}{L_{Te}} - \left(\frac{R}{L_{Te}}\right)^{cns}\right], \tag{35}$$

where the threshold gradient η_e^{cns} or $(R/L_{Te})^{cns}$ and the proportionality factors σ^{ns} all depend on the plasma parameters, such as τ_i, ε_n, $\hat{s}$ and q.

4.2. Negative magnetic shear

We consider the nominal negative magnetic shear $\hat{s} = -1$. The obtained critical gradient parameters η_e^{cns} and $(R/L_{Te})^{cns}$ are shown in Fig.3 for $\tau_i = 3$ (the line with solid squares), 2 (the line with open circles), 1 (the line with open squares), 1/3 (the line with solid circles). Here, the data points are the numerical results and the curves are from the fitting functions,

$$\eta_e^{cns} = \begin{cases} 6.549\varepsilon_n^2 - 1.199\varepsilon_n + 1.018, & \tau_i = 1/3, \\ 4.089\varepsilon_n^2 + 2.831\varepsilon_n + 0.6331, & \tau_i = 1, \\ 2.760\varepsilon_n^2 + 7.175\varepsilon_n + 0.3237, & \tau_i = 2, \\ 2.274\varepsilon_n^2 + 10.81\varepsilon_n + 0.1970, & \tau_i = 3, \end{cases} \tag{36}$$

and

$$\left(\frac{R}{L_{Te}}\right)^{cns} = \frac{\eta_e^{cns}}{\varepsilon_n}, \tag{37}$$

with η_e^{cns} given by Eq.(36). From Eq.(36) it is easy to find that $d\eta_e^{cns}/d\varepsilon_n > 0$ in the parameter regime studied here. We may also find that $(R/L_{Te})^{cns}$ decreases with ε_n for $\varepsilon_n < \varepsilon_n^0$. Here ε_n^0=0.4, 0.32, 0.3 and 0.25 for τ_i=1/3, 1, 2 and 3, respectively. Again, a higher τ_i is in favour of raising the threshold temperature gradient of ETG modes for $0.1 \le \varepsilon_n \le 0.6$. In addition, higher ETGs seem needed to drive the modes unstable in plasmas with peaked density profiles. In comparison with Ref.[7], we see that the threshold temperature gradient for a negative magnetic shear η_e^{cns} is

higher than the value for a positive magnetic shear of the same magnitude when the other parameters are also the same. For example, the critical $R/L_{\rm Te}$ values are 10 and 12 for $\hat{s}=1$ and $\hat{s}=-1$, respectively, when $\tau_{\rm i}=3$. For $\tau_{\rm i}=1$ these values are approximately 5 and 6 when $\varepsilon_n=0.2$.

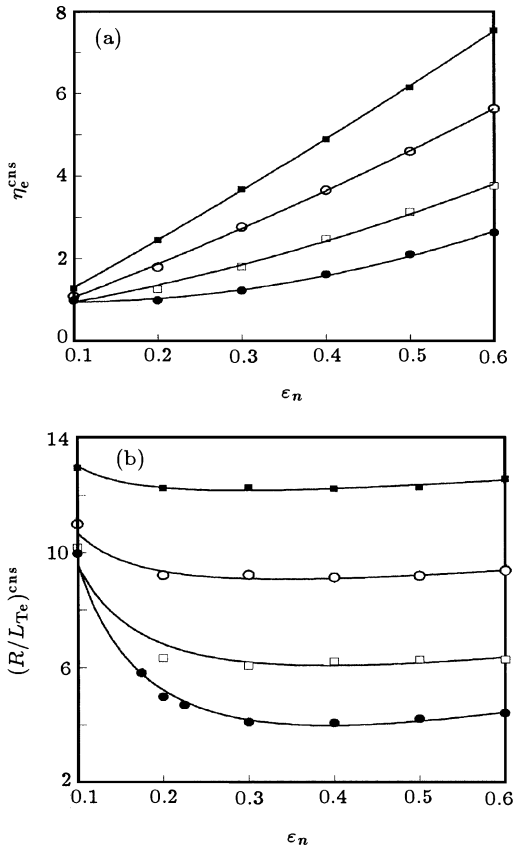


Fig.3. Critical gradient parameters $\eta_{\rm e}^{\rm cns}$ (a) and $(R/L_{\rm Te})^{\rm cns}$ (b) versus ε_n for $\hat{s}=-1$.

The coefficients in Eq.(36), depending on the parameter $\tau_{\rm i}$, may be expressed by polynomials. In this way, Eqs.(36) and (37) may be re-written as

$$\eta_{\rm e}^{\rm cns}=c_1^{\rm ns}(\tau_{\rm i})\varepsilon_n^2+c_2^{\rm ns}(\tau_{\rm i})\varepsilon_n+c_3^{\rm ns}(\tau_{\rm i}), \qquad (38)$$

and

$$\left(\frac{R}{L_{\rm Te}}\right)^{\rm cns}=c_1^{\rm ns}(\tau_{\rm i})\varepsilon_n+c_2^{\rm ns}(\tau_{\rm i})+\frac{c_3^{\rm ns}(\tau_{\rm i})}{\varepsilon_n},$$

where

$$c_1^{\rm ns}=0.794\tau_{\rm i}^2-4.18\tau_{\rm i}+7.74,$$
$$c_2^{\rm ns}=-0.603\tau_{\rm i}^2+6.47\tau_{\rm i}-3.21,$$

and

$$c_3^{\rm ns}=0.117\tau_{\rm i}^2-0.695\tau_{\rm i}+1.23.$$

The proportionality factor $\sigma^{\rm ns}(\varepsilon_n)$ in Eq.(34) is given in Fig.4, where the data points are from the numerical results and the symbols have the same meanings as those in Fig.3. Here, the curves are from the fitting functions,

$$\sigma^{\rm ns}(\varepsilon_n)=\begin{cases}1.45\varepsilon_n^2-0.288\varepsilon_n+0.0374, & \tau_{\rm i}=1/3,\\ 0.289\varepsilon_n^2+0.125\varepsilon_n-0.00567, & \tau_{\rm i}=1,\\ 0.0518\varepsilon_n^2+0.101\varepsilon_n-0.000795, & \tau_{\rm i}=2,\\ -0.0203\varepsilon_n^2+0.0968\varepsilon_n-0.0025, & \tau_{\rm i}=3.\end{cases} \qquad (39)$$

The definition of $\sigma^{\rm ns}$ in Eq.(35) leads to the essentially linear fitting functions in Eq.(39) for $\tau_{\rm i}$=2 and 3. The same procedure as for Eq.(36) may be carried out for the coefficients in Eq.(39) and results in

$$\sigma^{\rm ns}(\varepsilon_n,\tau_{\rm i})=g_1^{\rm ns}(\tau_{\rm i})\varepsilon_n^2+g_2^{\rm ns}(\tau_{\rm i})\varepsilon_n+g_3^{\rm ns}(\tau_{\rm i}), \qquad (40)$$

where

$$g_1^{\rm ns}(\tau_{\rm i})=-0.306\tau_{\rm i}^3+1.92\tau_{\rm i}^2-3.85\tau_{\rm i}+2.53,$$
$$g_2^{\rm ns}(\tau_{\rm i})=0.148\tau_{\rm i}^3-0.880\tau_{\rm i}^2+1.58\tau_{\rm i}-0.722,$$

and

$$g_3^{\rm ns}(\tau_{\rm i})=-0.0168\tau_{\rm i}^3+0.0979\tau_{\rm i}^2-0.171\tau_{\rm i}-0.0841.$$

Again, the maximum growth rate for a negative magnetic shear may be expressed as follows and used in future studies,

$$\gamma^{\rm max}=[g_1^{\rm ns}(\tau_{\rm i})\varepsilon_n^2+g_2^{\rm ns}(\tau_{\rm i})\varepsilon_n+g_3^{\rm ns}(\tau_{\rm i})]\omega_{*\rm e}\times\left\{\frac{R}{L_{\rm Te}}-\left[c_1^{\rm ns}(\tau_{\rm i})\varepsilon_n+c_2^{\rm ns}(\tau_{\rm i})+\frac{c_3^{\rm ns}(\tau_{\rm i})}{\varepsilon_n}\right]\right\}. \qquad (41)$$

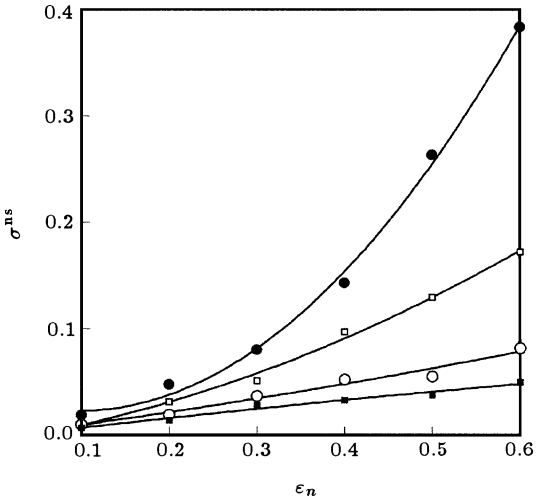


Fig.4. Proportionality factor $\sigma^{\rm ns}$ versus ε_n.

5. Conclusions and discussion

The experimental studies on electron temperature driven instabilities (ETG and trapped electron

modes) and the transport, from seven tokamaks devices (COMPASS-D, RTP, TCV, FT-U, AUG, Tore Supra and JET), have been reviewed in Ref.[11]. A great part of the experimental results were devoted to the determination of threshold gradient.

The experiments clearly show that there is a threshold of EGT, above which the transport increases strongly to keep the profiles unchanged. The experimentally measured threshold values lie between 8 and 12. The values given in Figs.2 and 3 are lower and close to the experimental observations. This shows that the experimentally measured $R/L_{\rm Te}$ may be determined by the ETG modes. Because the parameters ε_n, q, $\tau_{\rm i}$ and $\hat{s}$ for the experiments are not available, we do not attempt to claim the agreement of our results with the experiments. However, the fact that the theoretical results fall right inside the range of the experimental observations is certainly not an incidental event. At least, this is a strong support for the claim made in Refs.[11, 12] that the turbulence and turbulent transport observed in the experiments may be driven by the toroidal ETG modes.

Substituting Eq.(40) into Eq.(35), for negative magnetic shear, we have

$$\chi_{\rm e} \approx [g_1^{\rm ns}(\tau_{\rm i})\varepsilon_n^2 + g_2^{\rm ns}(\tau_{\rm i})\varepsilon_n + g_3^{\rm ns}(\tau_{\rm i})] \times \frac{ck_\theta^{\rm max}T_{\rm e}}{eBL_n}\left\{\frac{R}{L_{\rm Te}} - \left(\frac{R}{L_{\rm Te}}\right)^{\rm cns}\right\}, \quad (42)$$

where c is the speed of light, $k_\theta^{\rm max}$ is the poloidal wavevector corresponding to the maximum growth rate $\gamma^{\rm max}$, B and e are the magnetic field and the magnitude of electron charge, respectively.

Considering that the finite β effects are not significant for nowadays tokamak plasmas, as an approximation we may assume that $\Delta \approx c/\omega_{\rm pe} \approx 1/k_\theta^{\rm max}$, the collisionless skin depth, and make an estimation for the electron thermal transport coefficient,

$$\chi_{\rm e} \approx D_B[g_1^{\rm ns}(\tau_{\rm i})\varepsilon_n^2 + g_2^{\rm ns}(\tau_{\rm i})\varepsilon_n + g_3^{\rm ns}(\tau_{\rm i})] \times \frac{c}{\omega_{\rm pe}}\left\{\frac{1}{L_{\rm Te}} - \left(\frac{1}{L_{\rm Te}}\right)^{\rm cns}\right\} G^{\rm ns}(\hat{s},q) \quad (43)$$

for $L_{\rm T} \le L_{\rm Te}^{\rm cns}$, with $D_B = \dfrac{cT_{\rm e}}{eB}$ and $G^{\rm ns}(\hat{s},q)$ being the Bohm diffusion coefficient and an order unity function of the rest parameters, respectively.

In summary, the ETG-driven instability in toroidal plasmas in the parameter regime close to the stability boundary has been studied with gyro-kinetic theory in this work. The emphasis is placed on the calculations of the maximum growth rate and threshold temperature gradient of the modes. Direct calculation of the critical gradient is performed. The scaling of the maximum growth rate with ETG is given. The scaling of the critical gradient with the temperature ratio ($T_{\rm e}/T_{\rm i}$) and toroidicity (ε_n/R) is presented. The algebraic fitting formulae for the maximum growth rate and for the critical gradient are created from the numerical data. In addition, the critical temperature gradient (TG) in plasmas with negative magnetic shear $\hat{s}$ is higher than that with positive $\hat{s}$ when the other parameters and the magnitude of $\hat{s}$ are the same. This is also qualitatively in agreement with the experimental observations. The theoretical results for critical TG, obtained in this work, lie in the range of experimental results.

The quasi-linear estimations for electron thermal transport, with the collisionless skin depth as the correlation length given in this work may provide reference for future experiments and nonlinear simulations.

References

[1] Itoh K and Itoh S I 1996 *Plasma Phys. Control. Fusion* **38** 1

[2] Lee Y C, Dong J Q, Guzdar P N and Liu C S 1987 *Phys. Fluids* **30** 1331

[3] Guzdar P N, Liu C S, Dong J Q and Lee Y C 1986 *Phys. Rev. Lett.* **57** 2818

[4] Horton W, Hong B G and Tang W M 1988 *Phys. Fluids* **31** 2971

[5] Dorland W, Jenko F *et al* 2000 *Phys. Rev. Lett.* **85** 5579

[6] Jenko F, Dorland W *et al* 2000 *Phys. Plasmas* **7** 1904

[7] Jian G D and Dong J Q 2003 *Acta Phys. Sin.* **52** 1656 (in Chinese)

[8] Dong J Q, Sanuki H, Itoh K and Chen L 2002 *Phys. Plasmas* **9** 4699

[9] Jenko F, Dorland W and Hammet G W 2001 *Phys. Plasmas* **8** 4096

[10] Dong J Q, Jian G D, Wang A K, Sanuki H and Itoh K 2003 *Nucl. Fusion* **43** 1183

[11] Hoang G T, Bourdelle C, Garbet X *et al* 2001 *Phys. Rev. Lett.* **87** 125001

[12] Ryter F *et al* 2001 *Phys. Rev. Lett.* **86** 2325

[13] Ryter F *et al* 2001 *Phys. Rev. Lett.* **86** 5498

[14] Ryter F *et al* 2001 *Plasma Phys. Control. Fusion* A **43** 323

[15] Dong J Q, Horton W and Kim J 1992 *Phys. Fluids* B **4** 1867

[16] Sugama H 1999 *Phys. Plasmas* **6** 3527

[17] Dong J Q, Guzdar P N and Lee Y C 1987 *Phys. Fluids* **30** 2694